Soft-Chemistry-Assisted On-Chip Integration of Nanostructured α-Quartz Microelectromechanical System

Claire Jolly, Andres Gomez, David Sánchez-Fuentes, Dilek Cakiroglu, Raïssa Rathar, Nicolas Maurin, Ricardo Garcia-Bermejo, Benoit Charlot, Martí Gich, Michael Bahriz, Laura Picas, and Adrian Carretero-Genevrier*

The development of advanced piezoelectric α-quartz microelectromechanical system (MEMS) for sensing and precise frequency control applications requires the nanostructuration and on-chip integration of this material on silicon material. However, the current quartz manufacturing methods are based on bonding bulk micromachined crystals on silicon, which limits the size, the performance, the integration cost, and the scalability of quartz microdevices. Here, chemical solution deposition, soft-nanoimprint lithography, and top-down microfabrication processes are combined to develop the first nanostructured epitaxial (100)α-quartz/(100)Si piezoelectric cantilevers. The coherent Si/quartz interface and film thinness combined with a controlled nanostructuration on silicon–insulator–silicon technology substrates provide high force and mass sensitivity while preserving the mechanical quality factor of the microelectromechanical systems. This work proves that biocompatible nanostructured epitaxial piezoelectric α-quartz-based MEMS on silicon can be engineered at low cost by combining soft-chemistry and top-down lithographic techniques.

1. Introduction

Piezoelectric materials are at the core of many everyday applications, thanks to their intrinsic capability to generate electrical charges under applied mechanical stress or to induce a mechanical deformation from an electrical input. Such properties make them key elements of the motion detectors and resonators present in many wireless network sensors, which are the devices capable of harvesting and transmitting environmental data in an autonomous way. Thus, in this context, piezoelectric materials can find multiple military, security, medical, and environmental applications. Today, the monolithic integration of these materials into silicon technology and its nanostructuration to develop alternative cost-effective processes with superior performances are among the central points in current technology.[1,2] Generally, Pb[$Zr_x Ti_{1-x}$]O_3 ($0 \leq x \leq 1$) (PZT), ZnO, and AlN piezoelectric materials are integrated in the form of thin films on Si substrates for chip fabrication. By contrast, quartz-based devices have been so-far micromachined from bulk crystals. This has the disadvantages of limiting their downscaling to thickness below 10 µm[3,4] and that for most of their applications, quartz crystals need to be bonded on Si substrate.[5] These drawbacks represent an important bottleneck for the microelectronics industry, since the thinner single crystalline quartz plates are currently highly demanded over bulk structures for faster and higher frequency device operations as well as for their capability of lower detection levels with improved sensitivity.[4,6,7] Despite recent achievement to micropattern bulk crystals by laser interference lithography,[8] Faraday cage angled-etching, and focused ion beam,[4,9] the integration of thin patterned films on Si is still a challenge.

α-quartz is widely used as a piezoelectric material due to its outstanding properties.[5] While it can not be applied in energy harvesting applications because of its low piezoelectric coefficient, α-quartz presents an excellent chemical stability and high mechanical quality factor, which make it one of the best candidates for frequency control devices and acoustic sensor technologies.[10] Recently, we developed a direct bottom-up integration of epitaxial α-quartz into (100)silicon

C. Jolly, D. Sánchez-Fuentes, Dr. D. Cakiroglu, R. Rathar,
N. Maurin, Dr. R. Garcia-Bermejo, Dr. B. Charlot, Dr. M. Bahriz,
Dr. A. Carretero-Genevrier
Institut d'Electronique et des Systèmes (IES)
CNRS
Université de Montpellier
860 Rue de Saint Priest, Montpellier 34095, France
E-mail: carretero@ies.univ-montp2.fr

A. Gomez, Dr. M. Gich
Institut de Ciència de Materials de Barcelona ICMAB
Consejo Superior de Investigaciones Científicas CSIC
Campus UAB, Bellaterra, Catalonia 08193, Spain

Dr. L. Picas
Institut de Recherche en Infectiologie de Montpellier (IRIM)
CNRS UMR 9004–Université de Montpellier
Montpellier 34293, France

ADVANCED
SCIENCE NEWS
www.advancedsciencenews.com

ADVANCED
MATERIALS
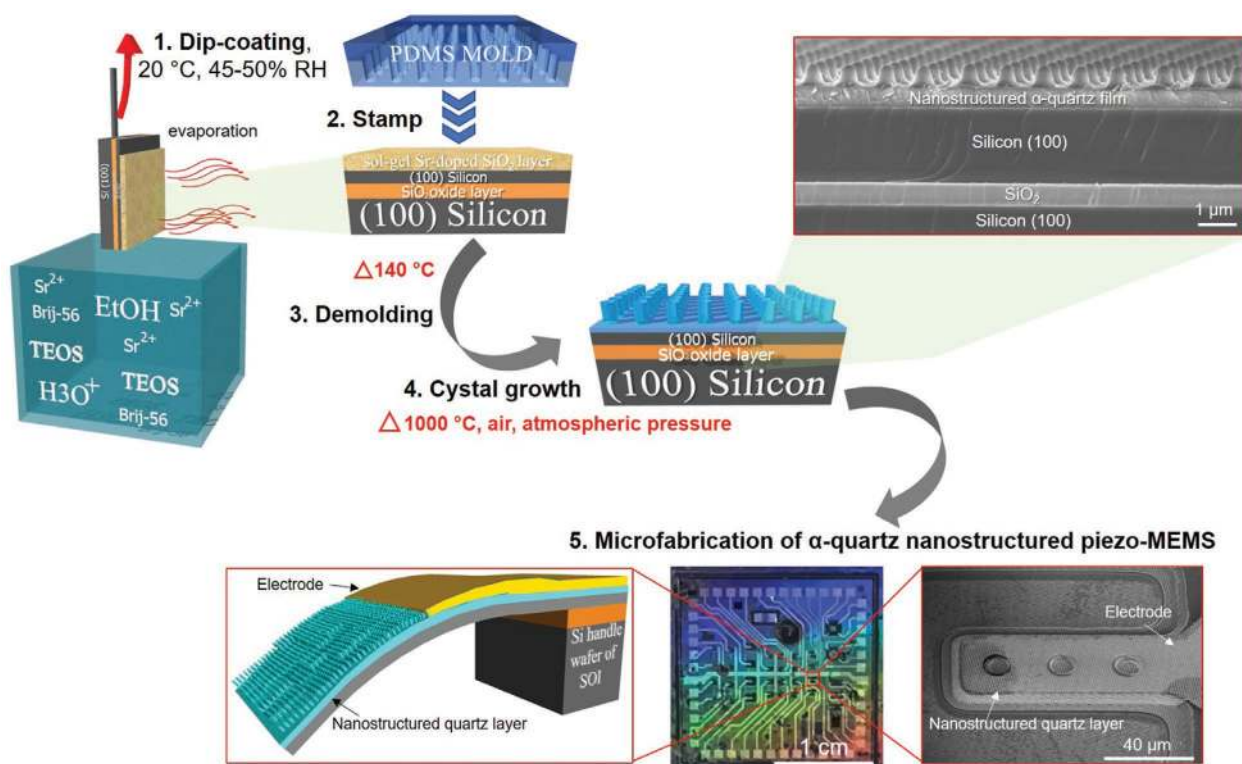**TECHNOLOGIES**
www.advmattechnol.de

Figure 1. General schematics of the synthesis and microfabrication of patterned quartz cantilever. Multilayer deposition of Sr–silica solution on SOI substrate by dip coating is followed by patterning of the film with NIL process. Annealing of the sample at 1000 °C enables the crystallization of nanostructured quartz film. Finally, a nanostructured quartz cantilever is fabricated. Notice that colored scattered optical image corresponds to the nanostructuration pattern on the surface of the device that is associated with the diffraction of natural light with the quartz nanopillars.

substrates.[11,12] Tailoring the structure of α-quartz film on silicon substrates was achieved by chemical solution deposition (CSD),[13] which allowed to control the texture, density, and the thickness of the films.[14] As a result, it is now possible to extend the available thicknesses of the α-quartz films from a few hundreds of nanometers to the micrometer range, which is 10–50 times thinner than those obtained by top-down technologies on bulk crystals. Moreover, optimization of the CSD conditions makes it possible to obtain a continuous crystalline quartz nanoimprinted pattern by a combination of a set of top-down lithography techniques.[15] Thus, this opens the possibility to develop cost-effective nanostructured piezoelectric epitaxial α-quartz-based microelectromechanical system (MEMS) with enhanced sensing properties.

In the present work, we report the fabrication of the first epitaxial piezoelectric nanostructured (100)α-quartz-/(100)Si-based cantilever, taking the advantage of the complementarity of soft-chemistry and top-down lithographic techniques combined with silicon–insulator–silicon (SOI) technology. We have engineered a coherent quartz/silicon interface with a quartz thickness above 1000 nm and a controlled nanostructuration, which enables the fabrication of sensitive on-chip quartz devices capable of measuring, thanks to its piezoelectricity, tiny forces, and masses through a variation in the resonance frequency while preserving the mechanical quality factor of the device. We also proved that the nanostructured quartz surface is biocompatible and induces the self-organization of proteins on cellular membranes. As a result, nanostructured quartz/Si MEMS could

be exploited for biosensing applications, for instance, to quantify a large number of cellular processes that are sensitive to surface topography (e.g., cell migration, membrane trafficking and signaling, and host–pathogen interactions), as previously reported on high-performance glass substrates.[16] Our results demonstrate the implementation of large-scale and cost-effective integration of nanostructured piezoelectric epitaxial quartz films into innovative electromechanical devices which can be used for future sensor applications in electronics, biology, and medicine.

2. Fabrication Steps of Nanostructured Piezoelectric α-Quartz-Based Cantilevers

In order to produce nanostructured quartz microcantilevers by silicon micromachining, we have engineered epitaxial nanostructured piezoelectric α-quartz films on (100) silicon–insulator–(100)silicon substrate, as illustrated in **Figure 1** (for extended data, see Figure S1a–e in the Supporting Information). The nanostructuration of (100)α-quartz surface films was performed by annealing nanoimprinted Sr–silica xerogel film deposited on (100)SOI substrate following the dip coating method previously reported.[15] Soft nanoimprint lithography (NIL) was applied on the last Sr–silica gel layer using a polydimethylsiloxane (PDMS) mold to pattern the film surface just before the whole quartz multilayer crystallization (see Figure S1c–e in the Supporting Information). Notice that

the nanostructuration process is not required to obtain a single crystal quartz layer. The thickness and density of the quartz film were controlled with the number of deposited layers, withdrawal rate, and humidity during synthesis, as previously described.[14] The final thickness of piezoelectric α-quartz films was set to 1200 nm, comprising a 600 nm thick quartz dense layer (i.e., the first three silica layers) and 600 nm thick nanopillared top surface with diameter and separation distances of 600 nm and 1 µm, respectively (last deposited silica layer) (see Figure S2 in the Supporting Information). The SOI substrate used along this work was composed of a 2 µm thick silicon active layer, a 500 nm thick silicon dioxide intermediate layer, and a 675 µm thick base. The piezoelectric activity of the epitaxial quartz films on SOI was evaluated by using the direct piezoelectric force microscopy (DPFM), a powerful methodology recently developed by the authors which allows to directly measure the piezoelectric effect in thin films.[17,18] Figure S3 (Supporting Information) shows that the piezoelectric coefficient obtained from these measurements is similar and comparable to that of quartz bulk materials (i.e., 1.5 and 3.5 pm V^{-1}).[19] Moreover, current profiles obtained from several consecutive spectroscopy experiments demonstrated a high level of homogeneity and reproducibility of epitaxial quartz films on SOI substrates. The crystallinity and crystal orientation of nanostructured α-quartz films were analyzed by 2D X-ray diffraction (2D XRD). Figure S4 (Supporting Information) shows a long range 2D θ–2θ XRD pattern of a 1200 nm thick patterned quartz film on SOI substrate, confirming the (100) out of plane texture of α-quartz with no supplementary peaks from other reflections or polycrystallinity signals. The rocking curve of the (100)quartz reflection presented in Figure S3b (Supporting Information) shows a mosaicity degree of 1.89°, as previously observed in films.[11]

We determined the optimal fabrication steps to produce nanostructured quartz-based cantilevers with a low cost and easy process on SOI substrate, as shown in Figure 1 and Figure S1 (Supporting Information). The key mechanistic aspects ensuring the preservation of the crystal quality, piezoelectric functionality, and mechanical quality factor, Q, of quartz-based cantilevers were i) the protection of the lateral edges of the patterned epitaxial quartz layer to avoid hydrofluoric acid (HF) infiltration during the release process of the cantilever (see Figure S1h, in the Supporting Information and the Experimental Section), ii) the use of a buffer HF solution for a gentle release of quartz-based chips, and iii) the increased thickness of the negative resist permitting longer wet etch times. As a result, quartz-based cantilevers present a coherent quartz/silicon interface with uniform epitaxial crystallinity and electromechanical properties, as further described in the following sections.

3. Structural and Electromechanical Characterization of Nanostructured Piezoelectric α-Quartz-Based Cantilevers

To confirm the crystallinity of the quartz layer after MEMS fabrication, 2D X-ray microdiffraction on a single cantilever was performed, as seen in **Figure 2**a. Figure 2b shows a tilted field emission gun scanning electron microscopy (FEG–SEM) image of a nanostructured quartz-based cantilever where the different crystalline layers observed in the 2D X-ray diffractogram are highlighted (i.e., (100) oriented epitaxial quartz layer that includes 600 nm thick quartz dense layer and 600 nm thick vertical nanopillared top surface, (100)silicon substrate, and the conformal polycrystalline 150 nm thick Pt electrode layer) (see also Figure S5 in the Supporting Information). The 2D XRD and rocking curve analysis revealed the same (100)quartz out of plane texture and full width at half maximum value that the films had before the microfabrication process (Figure 2g–i). Figure 2c–f displays a compositional analysis conducted by energy dispersive X-ray spectroscopy (EDX) elemental mapping. This analysis shows that the cantilever contains a homogeneous composition of Si, O, and Pt, which corresponds to the piezoelectric quartz layer and the top-electrode coating, whereas silicon is detected in the substrate as a unique element. Therefore, these results confirm the compatibility between MEMS fabrication process and material synthesis. The mechanical response of the quartz-based piezoelectric cantilevers was detected by using a laser Doppler vibrometer (LDV) equipped with a laser beam, a photodetector, and frequency generator (see Figure 2j and the Experimental Section for more information). Among the different cantilever's dimensions included in the fabricated chip (see Figure 1), the nanostructured cantilever analyzed in Figure 2j exhibited a rectangular geometry (40 µm wide and 100 µm long) and was fabricated with a 1200 nm thick patterned quartz layer. The measured resonance frequency was 267 kHz (comparable to similar commercial tip less cantilevers, see Figure S6 in the Supporting Information) and the estimated quality factor, Q, of the whole mechanical structure was $Q \approx 398$ under low vacuum conditions. This Q value of nanostructured quartz-based cantilevers is of the same order of magnitude as the mechanical Q of similar and standard non-piezoelectric silicon cantilevers which typically range from 50 to 1000, but can in some cases be as high as 10 000.[20] As a result, the epitaxial growth of (100) quartz layer on silicon might not affect the final mechanical Q value of the MEMS structure, probably due to the coherent quartz/silicon interface. Notice that this Q value depends on the external and internal damping phenomena, i.e., the cantilever geometry and the damping caused by viscous and other forces coming from the surrounding media.[21] Therefore, here we demonstrate the first, to our knowledge, cost-efficient on-chip integration of piezoelectric nanostructured epitaxial quartz-based MEMS. A comprehensive explanation of the methodology and reasoning employed for the calculation of quality factor of the nanostructured epitaxial quartz-based cantilevers can be found in the Supporting Information. We observed a linear dependence of cantilever displacement on the applied AC voltage. The inset of Figure 2f points out the linearity between the vibration amplitude and the actuation voltage at different AC voltages ranging from 1 to 10 V with 1 V increments. This shows that these devices can be activated through the converse piezoelectric effect coming from the epitaxial quartz layer.
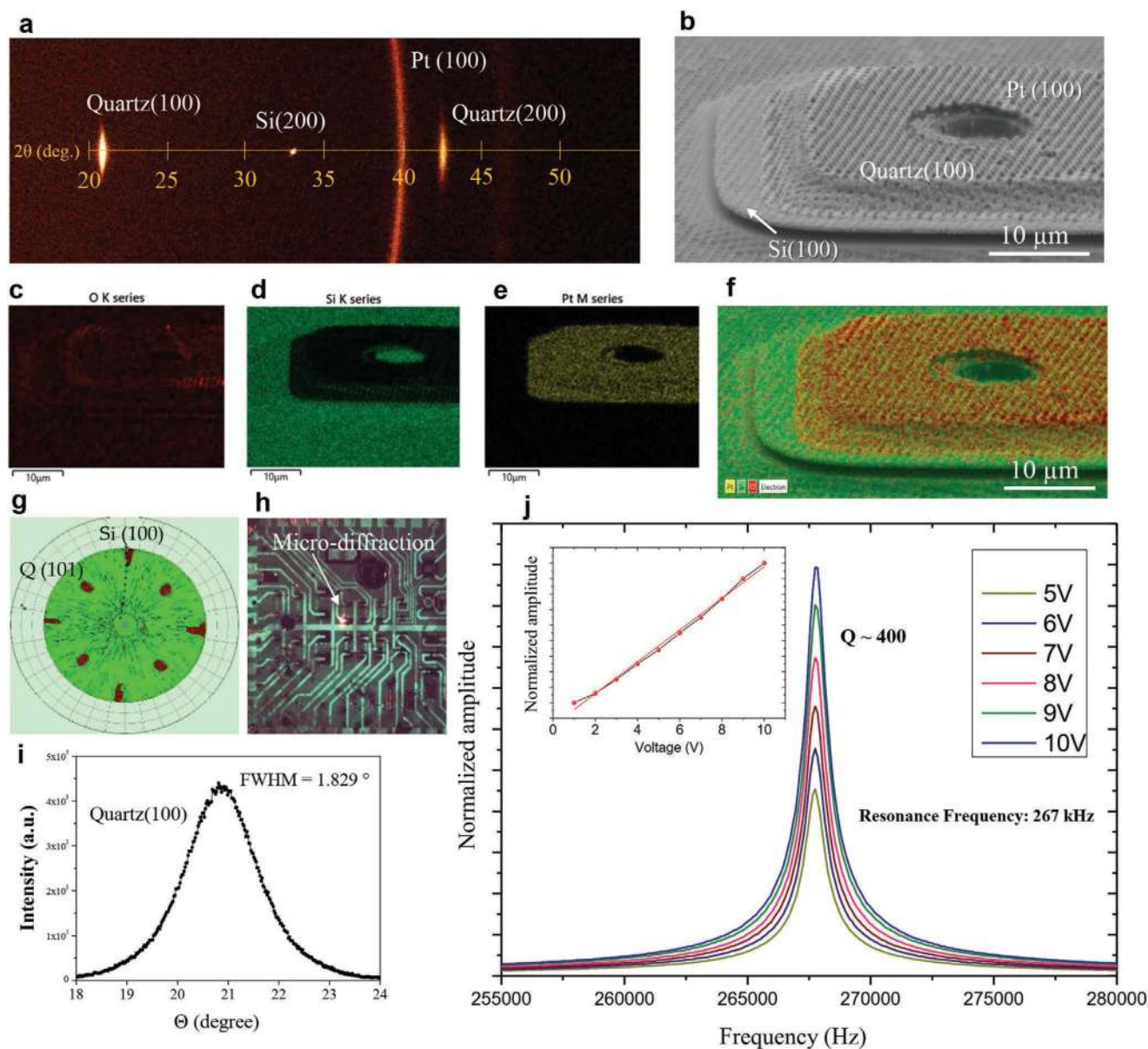
Figure 2. a) Crystallinity of the different materials present in the cantilever. Platinum used for contacts and (100) oriented quartz and silicon substrate are shown in the 2D XRD diffractogram. b) Tilted FEG–SEM image of nanostructured cantilevers showing the different layers of used material. c–f) Merch of tilted FEG–SEM image and chemical mapping of O, Si, and Pt elements of a single quartz/Si cantilever. g) 2D pole figure of nanostructured α-quartz(100)/Si(100) cantilever. h) Optical image of the whole chip during microdiffraction measurements at the zone pointed by a laser beam. Notice that the green color in the optical image corresponds to the diffraction of the natural light produced by the interaction of light and the quartz nanopillar which act as a photonic crystal. i) Rocking curve of the quartz/Si cantilever showing a mosaicity value of 1.829° of the (100) quartz reflection. j) Electromechanical characterization by noncontact vibrometry measurements under vacuum of a quartz-based cantilever 40 µm wide and 100 µm long composed of a 1200 nm thick patterned quartz layer. The nanopillar diameter and separation distance are 600 nm and 1 µm, respectively, and the thickness of the Si layer is 2 µm thick. The inset image shows the linear dependence of the cantilever amplitude on the applied AC voltage.

4. Electromechanical Characterization of Nanostructured α-Quartz Cantilevers by Atomic Force Microscopy (AFM)

The electromechanical properties of nanostructured quartz cantilevers were also studied under air condition by using AFM contact measurements. **Figure 3**a describes the working principle of AFM measurements, where an AC drive output of a lock-in amplifier (LIA) is fed to the top and bottom electrodes

of the cantilever, while the vibration is recorded with the optical beam deflection system of the AFM. Figure 3b,c shows the bulk oscillations of the AFM tip before and after routing the signals to the LIA's input, i.e., 0 and 10 V, respectively. These results show the active electromechanical response of the quartz-based microcantilevers, as already observed in the above described noncontact vibrometry measurements. Moreover, nanometric displacements as high as 12 nm under 10 V were observed, confirming that even under air conditions
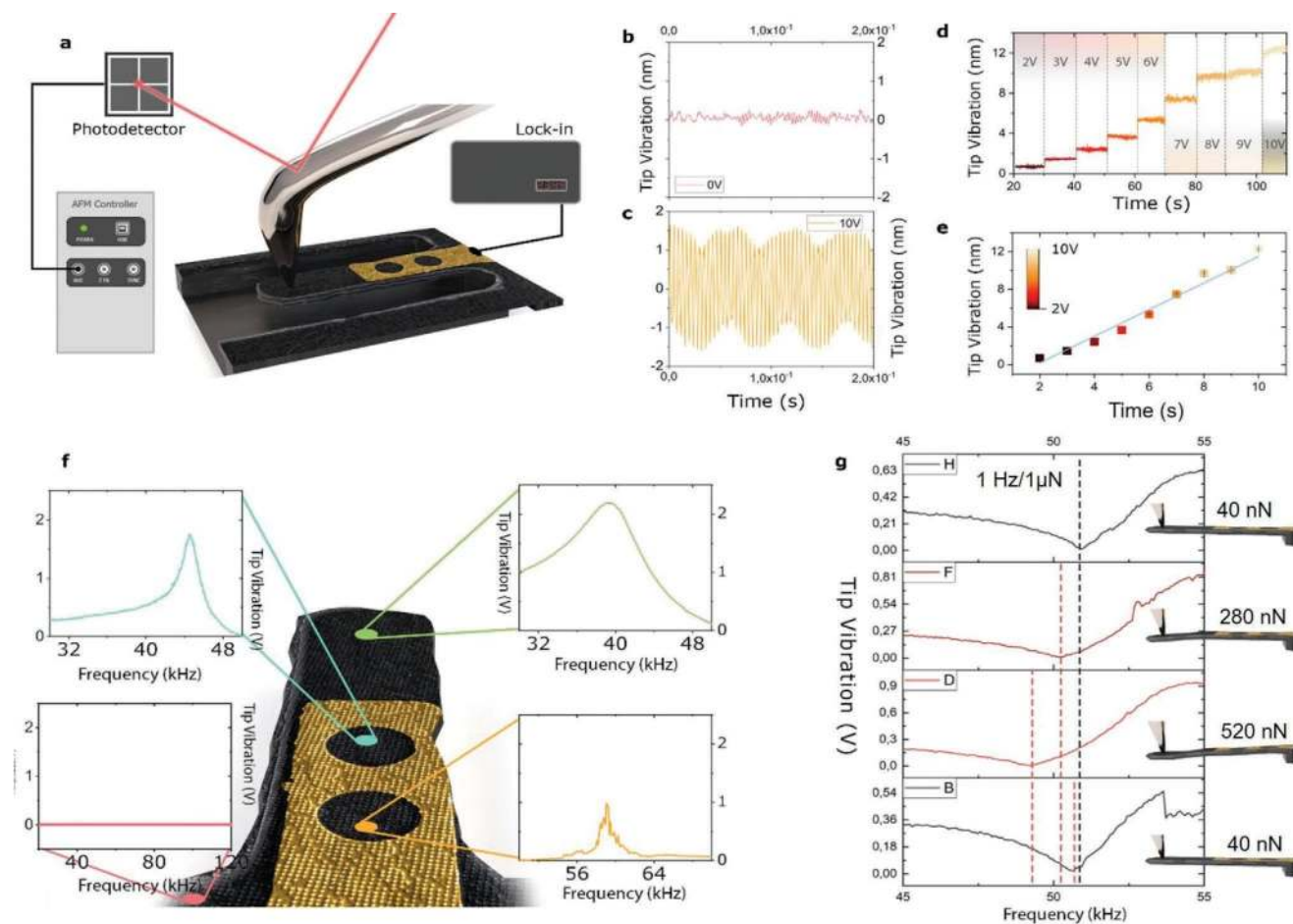
Figure 3. Characterization of quartz cantilevers using an atomic force microscope. a) The setup of the measurements in which the AC drive output of a lock-in amplifier is fed to the top (yellow zone) and bottom electrodes of the sample, while the vibration is recorded with the optical beam deflection system of the AFM. b,c) Bulk oscillations of the AFM tip before routing the signals to the LIA's input and after input 10 V signal, respectively. d,e) LIA's amplitude versus time for different applied voltage amplitudes (from 2 to 10 V AC). f) Resonance curves obtained from the combination of sample and tip spring constant in different spots of the cantilever. g) Evolution of the resonance frequency curve under different applied loads, starting from a low loading force of 40 nN till a maximum force of 520 nN. This calibration results in a sensitivity of 1 Hz/1 µN.

there is a robust mechanical coupling between the Si and the (100)epitaxial quartz layer actuated through the piezo-electric effect (see Figure 3d). This feature indicates that the quartz-based cantilever would not be much affected by the air damping phenomena and also by the clamping coming from the AFM tip that remains in contact on the surface of the quartz layer during the measurements. The same linearity between the vibration displacement and the actuation voltage was observed, therefore proving that these devices can be activated through the converse piezoelectric effect (see Figure 3e). Moreover, we discarded significant cantilever displacements due to electrostatic forces acting between the quartz-based cantilevers and the silicon surface. Accordingly, we performed electrostatic force microscopy experiments under the same conditions, voltage, surface, and separation distance to analyze the vibration of dimensionally similar commercial tipless silicon cantilevers. Figure S6 (Supporting Information) shows a residual vibration amplitude value of 0.04 nm under 10 V in a silicon tipless cantilever when it was separated by a similar distance as quartz cantilevers, i.e., 500 nm and from

the same chip surface. Therefore, we confirm that nanometric displacements observed in quartz-based microcantilever (12 nm under 10 V) at a separation distance of 500 nm from silicon surface were not induced by a capacitive phenomenon. We analyzed the resonance of the system (i.e., AFM tip and microcantilever) at different positions of the quartz-based microcantilever and as expected, the tip vibration amplitude increases closer to the end of the cantilever and disappears when the AFM tip is positioned out of the quartz-based resonator (see Figure 3f). Importantly, we have experimentally tested the mass and force resolution of nanostructured quartz-based cantilevers by applying different forces in the micronewton range with the AFM tip and recording in situ the resonance frequency evolution (see Figure 3g). Considering that Q higher than 100 allows for a frequency resolution below 10 Hz, we obtained a sensitivity of 1 µN Hz^{-1}, which results in a mass detection sensitivity of 100 ng Hz^{-1}. As a result, one could use commercial frequency modulators widely used in AFM microscopy, which display microhertz resolution, to resolve the masses in the picogram scale (see Figure 3g).
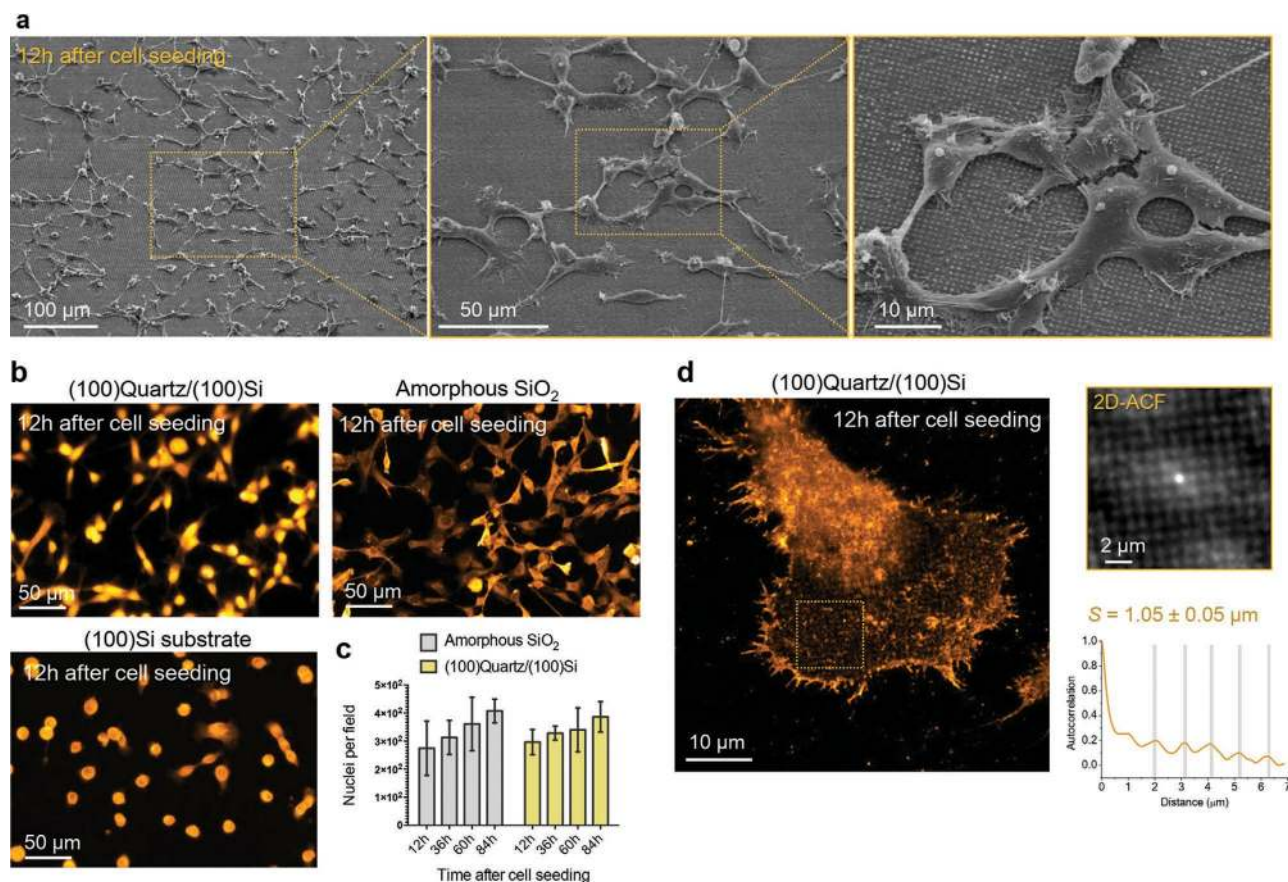
2000831 (5 of 9)

**ADVANCED
SCIENCE NEWS**
www.advancedsciencenews.com

**ADVANCED
MATERIALS
TECHNOLOGIES**
www.advmattechnol.de

Figure 4. a) Representative scanning electron microscopy images displaying HT1080 cells cultured on patterned (100)quartz/(100)Si during 12 h under culture conditions (37 °C and 5% CO_2). Scale bar, 10 and 5 µm for the magnified images. b) Representative widefield images of HT1080 cells expressing EGFR–GFP to visualize the cellular membrane. The same amount of cells was seeded on three different substrates: amorphous SiO_2 (which is the conventional substrate used in microscopy studies), (100)Si substrate, and patterned (100)quartz/(100)Si. Cells were cultured during 12 h before imaging. c) Quantification of the number of nuclei per field of image at different times (i.e., 12, 36, 63, and 84 h) after seeding HT1080 cells expressing EGFR–GFP on amorphous SiO_2 (gray) and patterned (100)quartz/(100)Si (yellow). Error bars represent standard deviation. d) Maximum intensity projection of a representative Airyscan image of HT1080 cells expressing EGFR–GFP and seeded on patterned (100)quartz/(100)Si substrates. 2D autocorrelation function and normalized autocorrelation curve of the EGFR signal corresponding to the orange dashed area indicated in the Airyscan image. Spacing (S) is indicated.

Because quartz-based devices are highly used for chemical and biosensing applications, such as quartz-crystal-microbalance-based setups,[7] we determined the biocompatibility of nanostructured α-quartz thin films engineered by chemical solution deposition, as detailed above (**Figure 4**). We confirmed that human epithelial cells, such as HT1080 cells, adhere and can be cultured on patterned epitaxial α-quartz thin films, as shown by scanning electron microscopy (see Figure 4a). Next, we compared the growth and proliferation of cells seeded on conventional glass coverslips typically used in biology studies with (100)quartz/(100)Si under cell culture conditions (37 °C and 5% CO_2). Whereas (100)Si substrate prevented proper adhesion of epithelial cells, we found that patterned (100)quartz/(100)Si and SiO_2 display equivalent biocompatibility, at least up to 84 h of under culture conditions, as shown by the quantification of the number of cells per field (N = 6) displayed in Figure 4b,c. Importantly, we found that nanostructured α-quartz thin films can induce the self-organization of the epidermal growth factor receptor (EGFR) on cellular membranes, as confirmed by the 1.05 µm spacing in the

2D autocorrelation function, which is in agreement with the PDMS mold used in this work (Figure 4d) and with previous studies using advanced fluorescence microscopy on borosilicate glass.[16] As a result, nanostructured biocompatible piezoelectric quartz-based MEMS could be applied for biosensing applications in the near future to quantify the contribution of surface topography on cellular processes such as cell migration, membrane trafficking and signaling, and host–pathogen interactions, among others.

Through this technology, these devices are expected to work also at the intrinsic quartz material frequency, which depends on the thickness of the quartz, i.e., around 10 GHz for a 800 nm thick resonator.[4] Operating at such high frequency avoids any damping and viscoelastic phenomena coming from the liquid environment, therefore decreasing the energy losses and improving the sensitivity. Moreover, the quality factor of the quartz material operating at this frequency is expected to be huge ($Q > 10^6$)[10] and not affected by the liquid damping. Since we obtained a sensitivity of 100 ng Hz^{-1}, we anticipate that quartz-based MEMS could

2000831 (6 of 9)

**ADVANCED
SCIENCE NEWS**

www.advancedsciencenews.com

**ADVANCED
MATERIALS
TECHNOLOGIES**

www.advmattechnol.de

be applied for cell mass detection. Indeed, the total mass of cells is ≈10 pg[22] and most of the experimental approaches for cell mass detection are typically based on either microfabricated resonators or optical methods.[23,24] Therefore, this new technology might overcome the bottlenecks and importantly, the limited working frequencies and sensitivity of the current quartz transducers made from bulk micromachining or hybrid integration methods, making possible to engineer a first nanoquartz balance with super mass resolution.

5. Conclusion

In conclusion, here we have combined a cost-effective and scalable chemical method with soft nanoimprint lithography and silicon micromachining to produce novel nanostructured epitaxial piezoelectric quartz-based microcantilevers. Using SOI technology, we have been able to modify the dimensions of piezoelectric quartz-based cantilevers while preserving a coherent (100)quartz/(100)silicon crystalline interface. Compared to the current production of quartz devices by top-down methods based on the miniaturization of large hydrothermally grown crystals, the soft-chemistry methodology allows obtaining thinner quartz layers on SOI substrates with thicknesses between 200 and 1000 nm and precise nanostructuration, which can generate piezoelectric patterned microdevices of different dimensions and designs. Noncontact vibrometry and contact PFM measurements of quartz-based MEMS activated by the piezoelectric effect revealed a nanoscale electromechanical motion in air and low vacuum. The coherent quartz/Si interface and the cantilever geometry gives rise to a Q value of 398 under low vacuum conditions, which is of the same order of magnitude as standard non-piezoelectric silicon cantilevers.

From a technological perspective, these novel quartz-based devices offer major advantages over quartz bulk in terms of size, power consumption, integration cost, and ability to provide multiple operation frequencies. This could pave the way to single chip solutions for multifrequency devices while preserving miniaturization and low-cost processes. Therefore, the described process could find applications in the field of electronics, medicine, or active biocompatible MEMS engineered from lead-free ferroelectric oxide materials. Indeed, we have proved the biocompatibility of nanostructured epitaxial quartz layers, which rendered cell adhesion and proliferation equivalent to that of conventional high-performance glass coverslips widely used in biology studies. As a result, biosensing applications to monitor the contribution of surface topography in cellular processes such as membrane trafficking and signaling and host–pathogen interactions should be possible in the near future due to the high sensitivity of nanostructured quartz cantilevers.

6. Experimental Section

Synthesis of Epitaxial Nanostructured Quartz Films: Nanostructured epitaxial (100)α-quartz film on (100)SOI substrate was prepared

combining two processes: multideposition of silica solution with dip coating and surface nanostructuration with soft lithography, NIL.

Solution Preparation: First, solution A was prepared by adding 0.7 g of Brij-58 into 23.26 g of absolute ethanol, then 1.5 g of HCl (37%), and 4.22 g of tetraethyl orthosilicate (TEOS). Mixture was stirred until the time it was used. Then, solution B was prepared with 1 M $SrCl_2 \cdot 6H_2O$ and water. Finally, solution C was prepared by adding 275 µL of solution B into 10 mL of solution A and stirred for 10 min. Sr–silica films were prepared with deposition of solution C onto SOI substrate by dip coating. It was suggested that every 40 min, new solution C should be prepared to preserve the stability of the deposited solution and also not to compromise the quality of the film. The amount of Sr introduced with solution B was such that, in solution C, the Sr/SiO_2 molar ratio was 0.05 and the final molar composition of $TEOS:Brij-58:HCl:EtOH:SrCl_2$ was 1:0.3:0.7:25:0.05.

Gel Film Deposition by Dip Coating: First, Sr–silica monolayer on SOI substrate was prepared by dip coating solution C with a 5 mm s^{-1} withdrawal rate in a controlled atmosphere. The ND-DC300 dip coater (Nadetech Innovations) equipped with an EBC10 Miniclima device allowed the deposition of Sr–silica at ambient temperature of 25 °C and relative humidity of 40%. After dip coating, the prepared gel film was consolidated with a thermal treatment for 5 min at 450 °C under the air atmosphere. The monolayer deposition process could be repeated many times depending on the desired film thickness.

Soft NIL Preparation (Preparation of Molds): Si masters used as molds in the NIL process were elaborated with different structures and heights using laser imprint lithography. PDMS reactants (90 wt% RTV141A, 10 wt% RTV141B from BLUESIL) were transferred onto the Si master and dried at 70 °C for 1 h before unmolding. Molds were degassed under vacuum (10 mbar) for about 20 min.

Nanostructuration of Film Surface with NIL: First, 500 nm of Sr–silica multilayer on SOI was prepared by repeating the monolayer deposition process. Then, one more monolayer was deposited on top of 500 nm of Sr–silica and this last layer was imprinted using PDMS mold without pressure. Peeling of PDMS mold was carried out after the prepared sample was placed in a furnace at 70 °C for 2 min and then at 120 °C for another 2 min to produce a column array of 600 nm height. Finally, the nanostructured sample was kept at 450 °C for 10 min for consolidation.

α-Quartz Crystallization: Nanostructured sample was introduced into the furnace at 1000 °C at atmospheric pressure and held at this temperature for 300 min for crystallization of quartz. Then, the sample was taken out of the furnace after the furnace was cooled down to room temperature.

Quartz Cantilever Microfabrication Process: On-chip integrated piezoelectric MEMS device which was designed and fabricated was the combination of the α-quartz thin film/nanopillar and metal electrodes on the SOI substrate purchased from Universal Wafer with a 2 µm thick silicon active layer, a 500 nm thick silicon dioxide intermediate layer, and a 675 µm thick base. In the design, the width and length of the rectangle-shaped cantilevers were 40 µm × 100 µm, 40 µm × 200 µm, and 36 µm × 70 µm, respectively.

The α-quartz piezoelectric cantilever was fabricated by microfabrication techniques. The fabrication process mainly included dry etching, top and bottom electrode deposition, and wet etching for cantilever releasing. All fabrication steps are shown in Figure S4 (Supporting Information). Before starting the fabrication process, all samples were cleaned in (2:1) $H_2SO_4:H_2O_2$ piranha solution for 10 min and rinsed with deionized water to get rid of the all organic residues on the sample surface.

Fabrication step started with defining the rectangular shape cantilever pattern on the quartz surface using a dry etching process. AZ2070 negative resist was used as an etching mask after EVG 620 UV lithography exposure. Quartz was etched until 2 µm silicon layer by inductively coupled plasma reactive ion etching (ICP-RIE) (model Corial 210 IL) using the $CHF_3/O_2/Ar$ gas mixture at 22 °C. End point detection and also two-point conductivity measurements were used to decide the etching time. The RIE conditions to engrave the sample were the following: 100 W radio frequency power, 200 W low frequency power, CHF_3 60 sccm/O_2 20 sccm/Ar 10 sccm at 32.5 Torr pressure.

The following step was to realize the top and bottom electrode. For this purpose, AZ2020 negative resist was spin coated on the sample surface and patterned using EVG 620 UV lithography for the 20 nm of Cr and 120 nm of Pt metal deposition. The top electrode was directly deposited on the top of the quartz and bottom electrode was deposited on the top of the 2 μm thick Si layer on SOI substrate. Fabrication step continued with etching 2 μm thick Si layer around the rectangular shape quartz structure using a dry etching process. In this step, the same etching procedure was followed as in the first step. In the final step, the quartz cantilever suspension from 675 μm Si base was released by a wet etching process. The 500 nm thick SiO_2 layer was etched by buffered hyrdofluoric acid BOE 7%. AZ2020 was used as an etching mask after 15 min of hard baking of the resist at 140 °C in order to strengthen the resilience against the acid.

Structural and Piezoelectric Characterization of Patterned Quartz Films and Cantilevers: The crystalline textures, rocking curve measurements, and epitaxial relationship of quartz films and cantilevers were performed on a Bruker D8 Discover diffractometer equipped with a 2D X-ray detector (3 s acquisition each 0.02° in Bragg–Brentano geometry, with a radiation wavelength of 0.154056 nm). The optical images of films and cantilevers were obtained in an Olympus BX51M optical microscope equipped with a Nikon DS-Fi3 camera. The microstructures of the nanostructured films and cantilevers were investigated with a FEG–SEM model Su-70 Hitachi, equipped with an EDX detector X-max 50 mm^2 from Oxford Instruments. The topography of nanostructured quartz films was studied by AFM in a Park Systems NX-Scanning Probe Microscopy unit. Piezoelectric characterization through the direct piezoelectric effect was made by direct piezoelectric force microscopy in an Agilent 5500LS instrument using a low leakage amplifier (Analog Devices ADA4530) with platinum solid tips (Rockymountain Nanotechnology RMN-25 PtIr200H). A periodically poled lithium niobate from the Bruker AFM was used as a reference testing platform.

Vibrometry Measurements: The vibration spectra of the fabricated quartz cantilever were evaluated by LDV equipped with laser, photodetector, and frequency generator. The vibrometer (OFV-500D, Polytech) was used in the displacement mode with a range of 50 nm V^{-1}. The frequency generator utilized to actuate the inverse piezoelectricity of quartz by the cantilever itself was an arbitrary waveform generator Agilent 33250A. The laser was an OFV-534, Polytech. The amplitude measurement of the fabricated quartz cantilever with a dimension of 40×100 μm was carried out under vacuum with the specific pressure of 2.6×10^{-2} mbar. The vibration spectra were initially obtained over a 100 kHz bandwidth to narrow the frequency window to be able to spot the resonance peak. Once it was found, the same short frequency sweep was performed to measure the vibration amplitude at different AC voltages.

Biocompatibility of Substrates and Cell Culture: HT1080 cells (a gift from N. Arhel and S. Nissole, IRIM, CNRS UMR 9004, Paris, France) were cultured in Dulbecco's modified Eagle medium GlutaMAX supplemented with 10% fetal calf serum and 100 U mL^{-1} of penicillin and streptomycin at 37 °C in 5% CO_2. Cells were tested negative for mycoplasma.

Endocytosis of functional EGFR–green fluorescent protein (GFP) was a gift from Alexander Sorkin (Addgene plasmid #32751). Plasmids were transfected 24 h after cell seeding using JetPEI transfection reagent (Polyplus transfection) according to the manufacturer's instructions.

Cells seeded on amorphous SiO_2, (100)Si, or patterned (100)quartz/(100)Si substrates were fixed in 3.2% paraformaldehyde in phosphate buffered saline (PBS) for 10 min at room temperature, then rinsed in PBS twice and incubated for 10 min at room temperature in 1% bovine serum albumin. Coverslips were then stained for Hoesch to reveal the cell nucleus. Finally, coverslips were mounted with a Mowiol 4-88 (Polysciences, Inc.).

For the quantification of cell growth and proliferation, images were acquired on a Zeiss Axioimager Z2 epifluorescent upright widefield microscope using a 20× Plan Apochromat 0.8 numerical apertures (MRI facility, Montpellier). Quantification was performed by using the nuclei staining (Hoesch) under ImageJ. Images for the analysis of protein self-organization at the cell surface were acquired on a Zeiss LSM880

Airyscan confocal microscope (MRI facility, Montpellier). Excitation source used was an argon laser of 488 nm wavelength. Acquisitions were performed on a 63×/1.4 objective. Multidimensional acquisitions were acquired via an Airyscan detector (32-channel GaAsP photomultiplier tube array detector).

Supporting Information

Acknowledgements

Conflict of Interest

The authors declare no conflict of interest.

Keywords

[1] D. Isarakorn, A. Sambri, P. Janphuang, D. Briand, S. Gariglio, J.-M. Triscone, F. Guy, J. W. Reiner, C. H. Ahn, N. F. de Rooij, *J. Micromech. Microeng.* **2010**, *20*, 055008.

[2] J. M. Vila-Fungueiriño, R. Bachelet, G. Saint-Girons, M. Gendry, M. Gich, J. Gazquez, E. Ferain, F. Rivadulla, J. Rodriguez-Carvajal, N. Mestres, A. Carretero-Genevrier, *Front. Phys.* **2015**, *3*, 38.

[3] W. R. Ali, M. Prasad, *Sens. Actuators, A* **2020**, *301*, 111756.

[4] Y.-I. Sohn, R. Miller, V. Venkataraman, M. Lončar, *Appl. Phys. Lett.* **2017**, *111*, 263103.

[5] J. S. Danel, G. Delapierre, *J. Micromech. Microeng.* **1991**, *1*, 187.

[6] B. Imbert, A. Reinhardt, T. Ricart, C. Billard, E. Defaÿ, H. Virieux, T. Jouanneau, F. Pierre, V. Delaye, P. Gergaud, E. Augendre, T. Signamarcheix, C. Deguet, S. Ballandras, *Joint Conf. of the IEEE Int. Frequency Control and the European Frequency and Time Forum (FCS) Proc.*, San Francisco, CA, USA **2011**, pp. 1–4.

[7] J. Rabe, S. Buttgenbach, J. Schroder, P. Hauptmann, *IEEE Sens. J.* **2003**, *3*, 361.

[8] Z. Santybayeva, A. Meghit, R. Desgarceaux, R. Teissier, F. Pichot, C. de Marin, B. Charlot, F. Pedaci, *J. Micro/Nanolith. MEMS MOEMS* **2016**, *15*, 034507.

[9] H. Lu, B. Sadani, N. Courjal, G. Ulliac, N. Smith, V. Stenger, M. Collet, F. I. Baida, M. P. Bernal, *Opt. Express* **2012**, *20*, 2974.

[10] S. Galliou, M. Goryachev, P. Abbe, X. Vacheret, M. Tobar, R. Bourquin, *IEEE Trans. Ultrason., Ferroelectr., Freq. Control* **2016**, *63*, 975.

[11] A. Carretero-Genevrier, M. Gich, L. Picas, J. Gazquez, G. L. Drisko, C. Boissiere, D. Grosso, J. Rodriguez-Carvajal, C. Sanchez, *Science* **2013**, *340*, 827.

[12] G. L. Drisko, A. Carretero-Genevrier, M. Gich, J. Gazquez, D. Ferrah, D. Grosso, C. Boissiere, J. Rodriguez-Carvajal, C. Sanchez, *Adv. Funct. Mater.* **2014**, *24*, 5494.

[13] A. Carretero-Genevrier, M. Gich, *JoVE* **2015**, *164*, e53543.

[14] Q. Zhang, D. Sánchez-Fuentes, A. Gómez, R. Desgarceaux, B. Charlot, J. Gàzquez, A. Carretero-Genevrier, M. Gich, *Nanoscale Adv.* **2019**, *1*, 3741.

[15] Q. Zhang, D. Sánchez-Fuentes, R. Desgarceaux, P. Escofet-Majoral, J. Oró-soler, J. Gázquez, G. Larrieu, B. Charlot, A. Gómez, M. Gich, A. Carretero-Genevrier, *ACS Appl. Mater. Interfaces* **2020**, *12*, 4732.

[16] T. Sansen, D. Sanchez-Fuentes, R. Rathar, A. Colom-Diego, F. El Alaoui, J. Viaud, M. Macchione, S. de Rossi, S. Matile, R. Gaudin, V. Bäcker, A. Carretero-Genevrier, L. Picas, *ACS Appl. Mater. Interfaces* **2020**, *12*, 29000.

[17] A. Gomez, M. Gich, A. Carretero-Genevrier, T. Puig, X. Obradors, *Nat. Commun.* **2017**, *8*, 1113.

[18] J. M. Vila-Fungueiriño, A. Gómez, J. Antoja-Lleonart, J. Gázquez, C. Magén, B. Noheda, A. Carretero-Genevrier, *Nanoscale* **2018**, *10*, 20155.

[19] R. Bechmann, *Phys. Rev.* **1958**, *110*, 1060.

[20] K. Naeli, O. Brand, *J. Appl. Phys.* **2009**, *105*, 014908.

[21] K. Yum, Z. Wang, A. P. Suryavanshi, M.-F. Yu, *J. Appl. Phys.* **2004**, *96*, 3933.

[22] U. Moran, R. Phillips, R. Milo, *Cell* **2010**, *141*, 1262.

[23] D. Martínez-Martín, G. Fläschner, B. Gaub, S. Martin, R. Newton, C. Beerli, J. Mercer, C. Gerber, D. J. Müller, *Nat. Methods* **2017**, *14*, 1129.

[24] T. Zangle, M. Teitell, *Nat. Methods* **2014**, *11*, 1221.